Two-Step Transformation of Aliphatic Polyketones into π-Conjugated Polyimines

Yumehiro Manabe,[†] Mitsuharu Uesaka,[†] Tomoki Yoneda,[†] and Yasuhide Inokuma*[†‡]

[†]Division of Applied Chemistry, Faculty of Engineering, Hokkaido University, Kita 13, Nishi 8 Kita-ku, Sapporo, Hokkaido 060-8628, Japan

[‡]Institute for Chemical Reaction Design and Discovery (WPI-ICReDD), Hokkaido University, Kita 21, Nishi 10, Kita-ku, Sapporo, Hokkaido 001-0021, Japan

KEYWORDS. polyketone • π-conjugation • polyimine • organic chromophore

ABSTRACT: The chemo- and stereoselective two-step transformation of aliphatic polyketones composed of 3,3-dimethylpentane-2,4-dione units was achieved to generate π-conjugated polyimines. Upon treatment with hydrazine, discrete oligoketones with 4–8 carbonyl groups afforded ethylene-bridged oligoisopyrazoles in 80–89% yields. These oligoisopyrazoles underwent stereoselective oxidation at the ethylene bridge to give fully π-conjugated oligo(isopyrazole-3,5-diyl-trans-vinylene)s in 73–87% yields. Oxidation of the oligoimines drastically changed their absorption and metal-coordination behaviors. Finally, this two-step transformation was applied to polydisperse polymers. Imine formation proceeded almost quantitatively, even for longer polyketones, including docosamer. Subsequent oxidation of the polyimines furnished a virtually insoluble material that showed broad and red-shifted solid-state absorption over the whole visible region resulting from extended π-conjugation.

INTRODUCTION

Aliphatic oligo- and polyketones are widely used as important precursors of polycyclic and aromatic compounds, and in engineering plastics.[1] An attractive features of these compounds is the diversity of chemical transformations using ketone-related reactions[2], with nucleophilic addition able to introduce various functional groups, and dehydrative condensation able to change the flexibility of the polyketone chains. These transformations are of particular importance in post-synthetic modifications used to induce drastic changes in the structural and optical properties of polyketones. However, chemo-, regio-, and stereoselectivity of such reactions to obtain structurally uniform and highly functionalized products is often problematic. For example, poly(1,4-diketone)s, which are common polyketones prepared from olefins and carbon monoxide, often contain isolated ketones after the Paal–Knorr-type conversion of 1,4-diketone units.[3] As a result, the final chemical structures become unclear, causing a decrease in the desired functionality. This implies that some knowledge gaps remain between controlled transformations of small molecules and macromolecules with proper structural elucidation. Therefore, reliable chemical transformation methods are needed.

Recently, our group developed a new polyketone sequence composed of alternating 1,3- and 1,4-diketones from the oligomerization of 3,3-dimethylpentane-2,4-dione (**1**).[4] Unlike other polyketone sequences, oligomers of **1** underwent highly chemoselective transformations. Upon treatment with acid, only the 1,4-diketone units were converted into furan rings, while reactions with hydrazine resulted in the formation of isopyrazole rings from 1,3-diketone subunits. Furthermore, such chemically modified chains exhibited unique structural and metal-coordination characteristics to form two- and three-dimensional assemblies. These features prompted us to further investigate the chemical functionalization of polyketones to induce dramatic changes in structural and optical properties.

Herein, we report the two-step synthesis of π-conjugated polyimines from poly(3,3-dimethylpentane-2,4-dione)s. These chemical conversions generated structurally rigid organic chromophores from flexible and non-conjugated compounds. We first examined the transformation reactions of discrete oligomers **4**–**6** to optimize the reaction conditions and to investigate the resulting changes in optical and structural properties in detail. We found that condensation reactions between hydrazine monohydrate and oligoketones proceeded quite efficiently under mild conditions to give ethylene-bridged isopyrazole oligomers **7**–**9**. Subsequent oxidation of **7**–**9** with *p*-chloranil converted the bridging ethylene units into *trans*-vinylene groups to afford multiple nitrogen-embedded all-*trans* polyene derivatives **10**–**12**. The structures of these discrete oligomers were fully determined by NMR, ESI–TOF MS, and single crystal X-ray diffraction analyses. UV–Vis

absorption spectra and DFT calculations confirmed that the lowest energy transition bands of the oligomers were redshifted with an increasing number of repeating units. Changes in the structural flexibility upon oxidation of the imine chains also altered the coordination behavior with Cd^{2+} ions. Finally, we applied the two-step transformation protocol to polydisperse polymer **15**. Even for longer analogues, the condensation reaction with hydrazine proceeded completely to give polyimines **16**. Subsequent oxidation afforded π-conjugated organic chromophore **17** with a small HOMO–LUMO gap.

RESULTS AND DISCUSSION

Oligo(3,3-dimethylpentane-2,4-dione)s **4**–**6** used in this study were prepared by the silver(I) oxide mediated oxidative coupling of corresponding enol silyl ethers (Scheme 1). By changing the base and solvent, mono- and bis-silyl enolates **2**[4] and **3**[5] were exclusively obtained from **1** in 93% and 80% yields, respectively, according to reported procedures. While dimer **4** was prepared by homocoupling reaction of silyl enolate **2**, trimer **5** was synthesized from the cross-coupling reaction between **2** and **3** under similar silver(I) oxide mediated reaction conditions.[4,6] When precursors **2** and **3** were used in a 2.2 : 1 molar ratio, trimer **5** was formed in only 11% yield based on compound **3**, along with other oligomers such as **4** (23%) and **6** (14%). In the presence of excess **2** (5 equiv.), the formation of longer oligomers was suppressed and trimer **5** was isolated in 27% yield based on **3**. Tetramer **6** was also synthesized using a previously reported procedure, but using ethyl acetate instead of diethyl ether as the extraction solvent, which gave a slightly increased isolated yield of **6** (55%).

With the aim to changes the structural and optical properties of polyketone chains through chemical transformations, we attempted to generate extended π-conjugation over the main carbon chains of **4**–**6**. To circumvent the quaternary carbon atoms (dimethylmethylene subunits), we planned to create linear π-conjugation by oxidizing the main chain after converting the 1,3-diketone subunits into isopyrazole rings (Scheme 2).

The condensation reaction of oligoketones **4**–**6** with hydrazine monohydrate[4,7] proceeded under mild conditions to give ethylene-bridged isopyrazoles **7**–**9** in 80–89% yields. Although t aqueous workup caused slight loss of the hydroscopic products **7**–**9**,[8] ^{1}H NMR analysis of the reaction solution confirmed virtually quantitative condensation of **4**–**6** without the formation of detectable byproducts. The complete disappearance of carbonyl groups after treating with hydrazine was also confirmed by $^{13}C\{^1H\}$ NMR analysis, with no signals observed in the carbonyl region (200–210 ppm) and imine carbon peaks observed at 180–190 ppm.

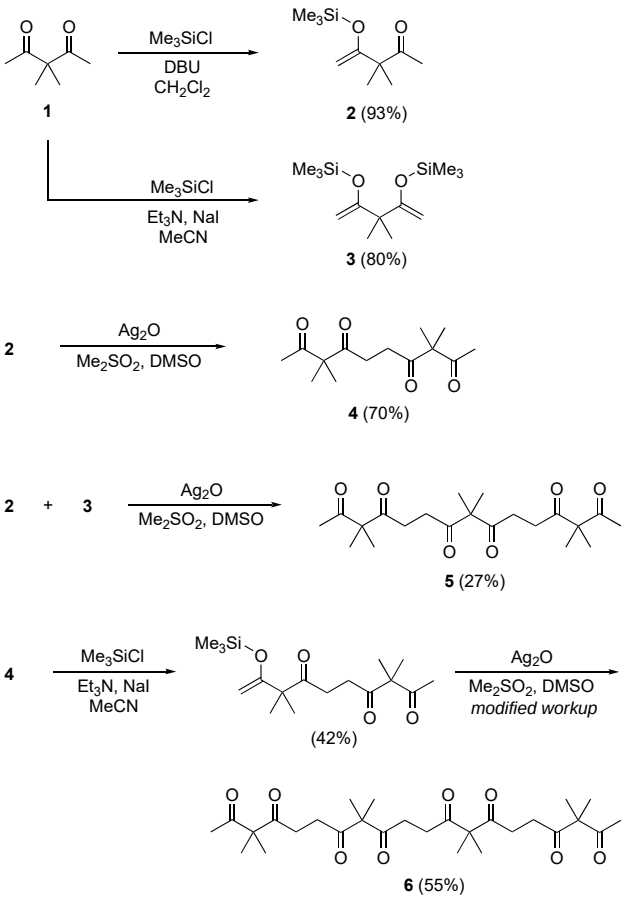

Scheme 1. Synthesis of discrete oligoketones **4–6.**

Ethylene-bridges in oligoimines **7**–**9** were completely and stereoselectively oxidized to *trans*-vinylene units upon oxidation with *p*-chloranil in 1,4-dioxane.[9] When diisopyrazole **7** was treated with *p*-chloranil (1.1 equiv.) at room temperature, compound **7** was completely consumed in 1 h. Reaction monitoring by ^{1}H NMR spectroscopy showed that the olefinic proton peak at 7.27 ppm appeared concomitantly with the decrease in the ethylene proton signal at 2.98 ppm without forming detectable side products. After chromatographic purification, oxidized product **10** was isolated in 87% yield as an off-white solid. Under similar reaction conditions, compound **8** gave conjugated isopyrazole **11** in 78 % yield. Although the oxidation reaction of tetramer **9** was not completed at room temperature presumably due to the low solubility of reaction intermediates (*i.e.* partially oxidized products), product **12** was obtained in 73% yield when the reaction solution was heated to 50 ºC. The terminal vinylene proton signals (7.41 and 7.32 ppm, and 7.41 and 7.33 ppm in $CDCl_3$ for **11** and **12**, respectively) were observed as a pair of doublets with a coupling constant of 17.0 Hz, which indicated *trans*-selective oxidation. Notably, even for the oxidation of tetramer **9**, diastereomers, namely *cis*-vinylene isomers, were not observed.

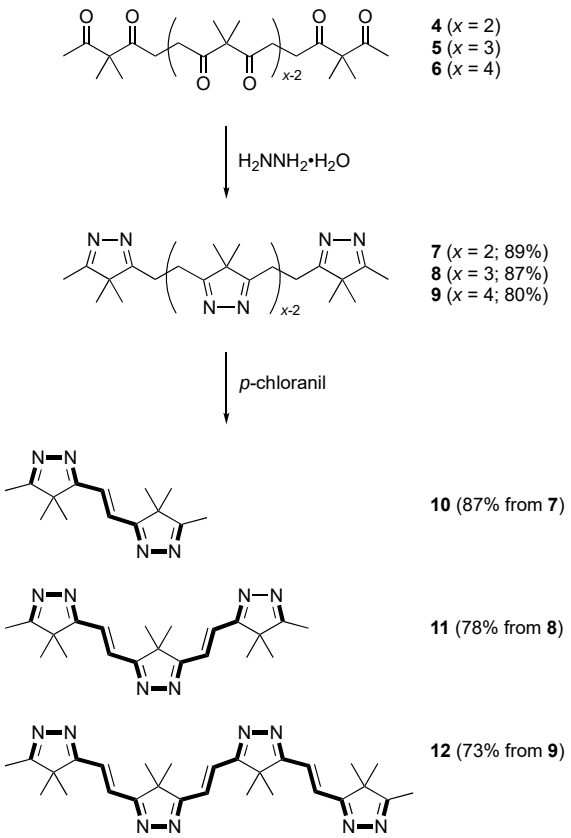

Scheme 2. Two-step transformation of oligoketones **4–6** into conjugated imines **10–12.**

Single crystal X-ray analysis unambiguously confirmed the *trans* configuration of the vinylene-bridge in compounds **10** and **11** (Figure 1).[10,11] The C=C double bond lengths were 1.339(3) Å (C5=C5') for **10** and 1.346(2) Å (C5=C6 and C5'=C6') for **11**. In the crystal, the diazadiene subunits (N2=C4–C5=C5' and N2'=C4'–C5'=C5) of **10** both adopted s-*trans* conformations. Similarly, compound **11** was observed to have an all-s-*trans* conformation. The planar structures of **10** and **11** were indicative of the effective extension of π-conjugation over the oligoimine chains. Although parent oligoketones **4–6** show curled or waved structures in the carbon main chains (see SI and ref. 4), the X-ray structures of **10** and **11** suggested rather rigid and rod-like conformations for the conjugated imines. This implied that the structural flexibility of the carbon chains was markedly altered by the two-step transformation. In fact, oxidized products **10–12** became less soluble in common organic solvents, such as DMSO, toluene, and acetonitrile, as the number of repeating subunits increased, while parent carbonyl and imine compounds **4–9** retained good solubility regardless of the chain length.

Oxidation of the ethylene bridges in oligoimines **7–9** to give conjugated imines **10–12** led to drastic changes in the UV–Vis absorption spectra (Figure 2). While oligoketones **4–6** and oligoimines **7–9** did not show any absorption band above 300 nm in CH_2Cl_2, an intense absorption band with a molar extinction coefficient of 2.2×10^4 L mol^{-1}cm^{-1} was observed at λ_{max} = 309 nm for conjugated dimer **10**. The lowest energy absorption band was redshifted to 363 and 392 nm in **11** and **12**, respectively, accompanying with the increased absorption coefficient. As a result of the bathochromic shift, compounds **11** and **12** exhibited a yellow color in solution (see SI). This tendency was similar to those of polyenes and their nitrogen-embedded analogues, such as azines.[12] The UV–Vis absorption spectra clearly showed that π-conjugation was extended by oxidation of the ethylene bridges, despite the presence of quaternary carbons in the main chains.

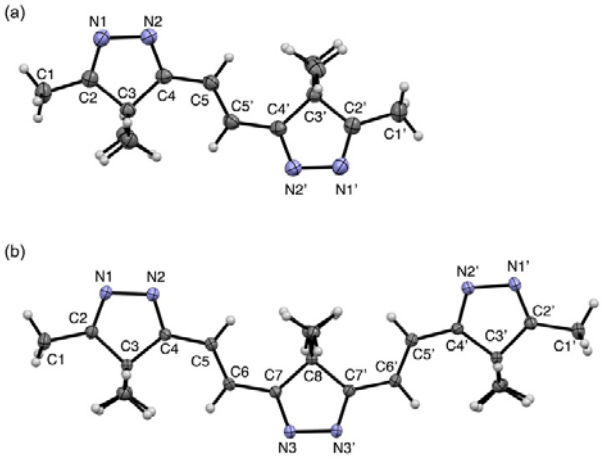

Figure 1. X-ray crystal structures of conjugated oligoimines (a) **10** and (b) **11**. Selected bond lengths (Å): N1–N2 1.4421(17), N2–C4 1.2919(18), C4–C5 1.449(2), C5–C5' 1.339(3) for **10**; N1–N2 1.4487(18), N2–C4 1.297(2), C4–C5 1.453(2), C5–C6 1.346(2), C6–C7 1.452(2), C7–N3 1.302(2), N3–N3' 1.436(2) for **11**.

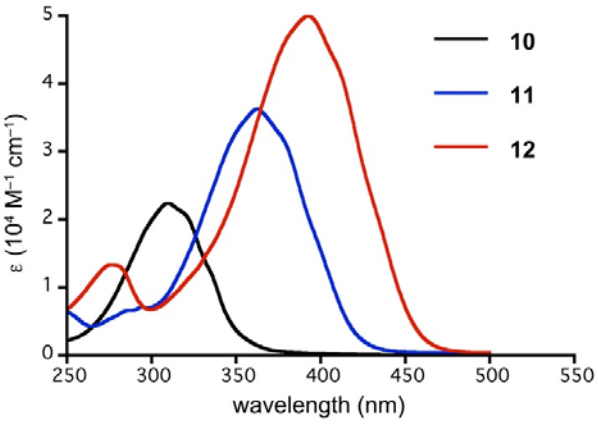

Figure 2. UV–Vis absorption spectra of conjugated imines **10–12** in CH_2Cl_2.

The metal coordination behavior of isopyrazole subunits in oligoimine chains also dramatically changed upon oxidation of the ethylene bridge. In a previous study, we have

reported that structures of metal complexes with tetraimine ligand **7** varied depending on the metal ions and stoichiometry owing to their structurally flexible nature.[4,13] When isopyrazole dimer **7** was complexed with $Cd(NO_3)_2•4H_2O$ in acetonitrile, colorless crystals formulated as $[Cd(\mathbf{7})_2(OH_2)_2(NO_3)_2•(CH_3CN)]_n$ (**13**), were obtained in 44% yield (Scheme 3a). The two-dimensional coordination network structure of complex **13** was determined by single crystal X-ray analysis.[14] Each ligand **7** was coordinated to two different Cd^{2+} ions through the terminal iminic nitrogen atoms as a bidentate bridging ligand, while two internal nitrogen atoms remained uncoordinated (Figure 3). This type of coordination is essentially the same as that previously reported for the Zn complex of **7**[4].

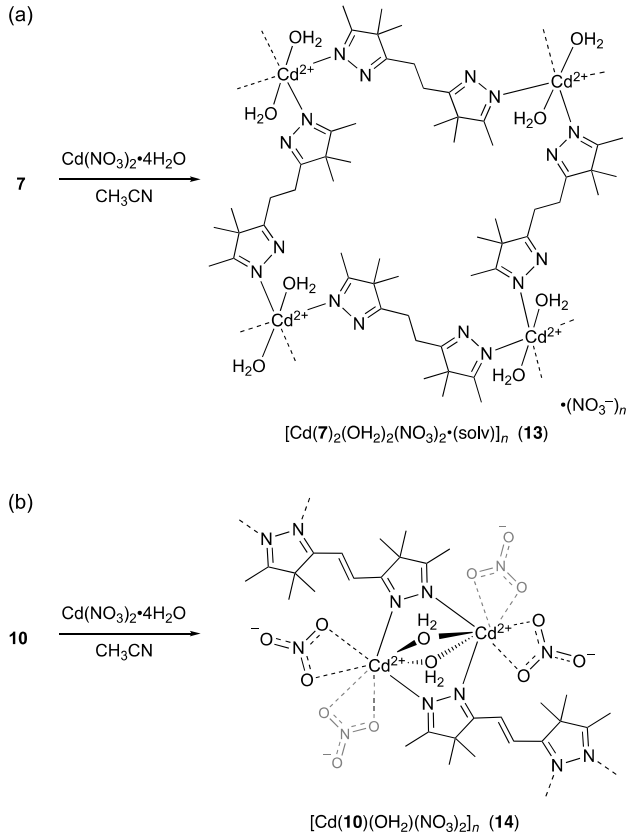

Scheme 3. Complexation of $Cd(NO_3)_2•4H_2O$ with (a) ligand **7** and (b) **10.**

Oxidized compound **10** gave a different Cd complex $[Cd(\mathbf{10})(OH_2)(NO_3)_2]_n$ (**14**) in 37% yield as microcrystals under similar conditions (Scheme 3b). Single crystals of **14** for X-ray diffraction analysis were grown from ethanol.[15] The crystal structure of **14** showed the repeating di-μ-isopyrazole-di-μ-aquo-tetrakis(nitrato-*O*,*O*')dicadmium substructures[16] that were one-dimensionally linked by *trans*-vinylene bridges to form coordination polymers.[17] Ligand **10** adopted an all s-*trans* conformation similar to its pure form. Unlike complex **13**, all the nitrogen atoms in ligand **10** were coordinated by four different Cd^{2+} ions. The difference in the coordination behavior of **7** and **10** with Cd^{2+} ions was attributed to the lower steric hinderance of the favored s-*trans* conformation of **10** during metal coordination to the internal nitrogen atoms.

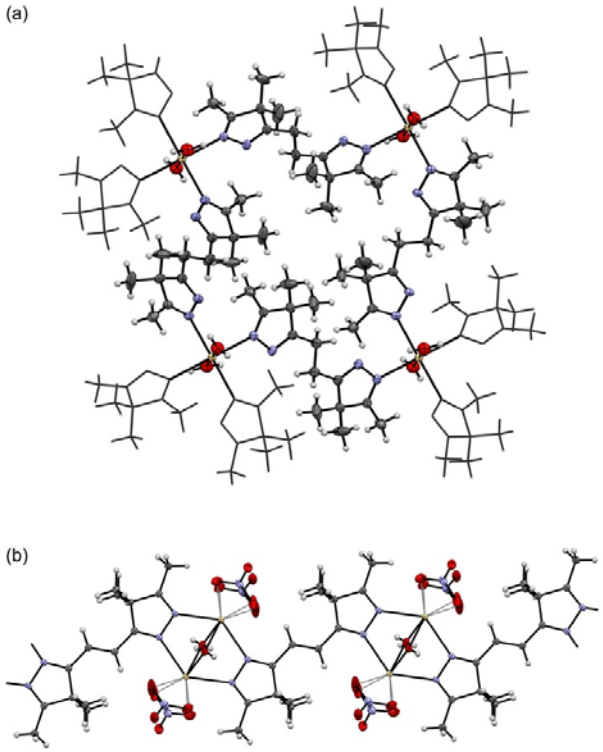

Figure 3. X-ray crystal structures of (a) coordination network **13** and (b) coordination chain **14**. Thermal ellipsoids are set at the 50% probability level. (gray: carbon, sky blue: nitrogen, red: oxygen, yellow: cadmium, and white: hydrogen)

Encouraged by the efficient two-step transformation of oligoketones **4**–**6** and attractive changes in structural and optical properties, we examined similar conversions of polydisperse polymers. When bis-silyl enolate **3** was exposed to homocoupling conditions, polymer **15** with a mean degree of polymerization of 5.1 was obtained in 64% yield (Scheme 4). MALDI TOF–MS analysis of **15** showed ion peaks of up to the docosamer (22-mer) in the Na^+ ion adduct form (see SI), and the polydisperse index of **15** was estimated to be 1.24. Treatment of polymer **15** with hydrazine monohydrate (1.2 equiv. based on monomer units) in THF resulted in the complete disappearance of carbonyl carbon signals at 207.7–209.6 ppm. Instead, signals assigned to imine carbon atoms were observed at 180.3–182.2 ppm. After a workup similar to that applied to oligomers, polyimine **16** was obtained in 94% yield. MALDI TOF–MS spectrum of **16** also indicated complete conversion of the 1,3-diketone units into isopyrazoles.

Upon treatment of polyimine **16** with *p*-chloranil in 1,4-dioxane under reflux, the reaction solution immediately turned dark brown, and a precipitate was formed. Although shorter oligomers (from dimer **10** to tetramer **12**) were extracted by washing the precipitate with dioxane and methanol, most part of the precipitate was insoluble in

common organic solvents, suggesting the formation of structurally rigid products with extended π-conjugation.

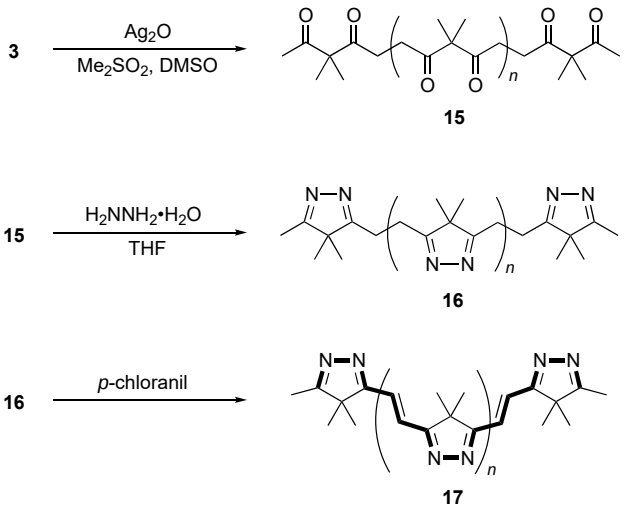

Scheme 4. Synthesis of polyketone **15** and its transformation into conjugated polyimine **17.**

IR spectroscopy suggested efficient oxidation of the ethylene bridges in polymer **16**. Before the oxidation, dimer **7** exhibited imine stretching signals at 1572 cm^{-1} as nearly a single band. After oxidation, conjugated imine **10** showed two different signals for imine stretching modes at 1566 and 1523 cm^{-1}, which were assigned to stretching bands of the terminal and *trans*-vinylene-bridged internal imines, respectively. A similar tendency was observed for trimers **8** and **11**, and tetramers **9** and **12**, while the relative intensities of the conjugated imine at 1513 cm^{-1} (for both **11** and **12**) were enhanced as the number of imine subunits increased. For the polymers, although the IR spectrum of non-conjugated polyimine **16** was similar to that of oligomers **7**–**9**, conjugated polyimine **17** exhibited very weak signals for the terminal imines at 1568 cm^{-1}. Instead, an intense signal corresponding to internal imines was observed at 1510 cm^{-1}. Considering that the mean degree of polymerization of parent polyketone **15** was 5.1, this strongly suggested that ethylene-bridges in polyimine **16** were quite efficiently oxidized.

Solid state diffuse reflectance spectroscopy confirmed the drastic extension of π-conjugation in oxidized polymer **17** (Figure 4). Broad absorption bands of **17** (λ_{max} = 414 nm) covered the whole visible region and the absorption edge reached the near infrared region (~900 nm). Compared with tetramer **12**, the bathochromic shift in the absorption spectrum was notable, which indicated very long-range π-conjugation in polymer **17**.

DFT calculations were performed to further investigate the effect of π-conjugation extension. Geometry optimization was conducted at the B3LYP/6-31G* level using the coordinates of the crystal structures of **10** and **11**, and all *trans*-vinylene and s-*trans* conformations for **12** and longer oligomers (hexamer, octamer, dodecamer, and hexadecamer as initial structures; see SI). For all oligomers, planar conformations were obtained as the optimized structures. Comparing the energy levels for frontier orbitals clearly showed that the HOMO–LUMO gaps gradually decreased as the number of repeating subunits increased (Figure 5a). While marked stabilization of the LUMO energy level was observed up to the octamer, shifts in the HOMO and LUMO levels were trivial for longer oligomers.

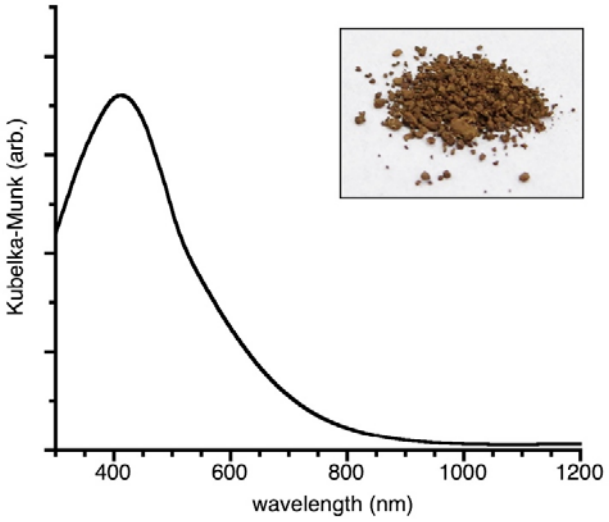

Figure 4. Diffuse reflectance spectrum of conjugated imine polymer **17**. Inset shows the picture of polymer **17** under ambient light.

The Kohn–Sham orbitals for HOMOs and LUMOs of **10**–**12** were reminiscent of those in polyenes (Figure 5b). For the 10π-electron system of compound **10**, four and five nodal planes were found in the HOMO and LUMO, respectively, as observed for decapentaene analogues.[18] As the number of π-electrons increased, the number of nodal planes in the frontier orbitals for compounds **11** and **12** also increased, to seven and ten nodes for the HOMOs of **11** and **12**, respectively. While a similar tendency was observed for longer oligomers, the orbital coefficients at the terminal isopyrazole subunits became negligible. This implied that the effective conjugation length was limited, even as the number of subunits increased, as suggested by the energy level shifts in the HOMOs and LUMOs.

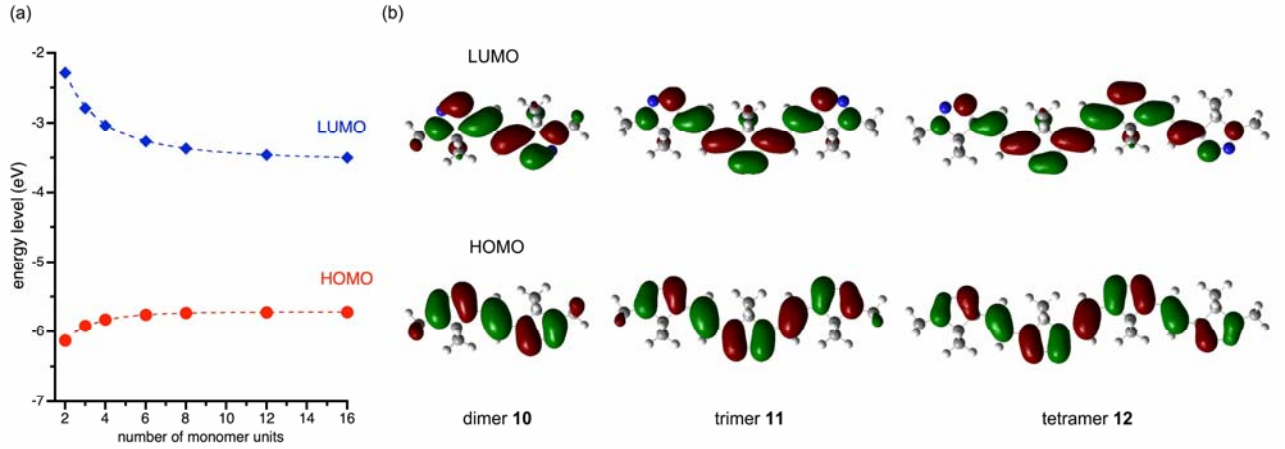

Figure 5. (a) Energy levels of frontier orbitals for conjugated oligoimines **10**–**12**. (b) Kohn–Sham orbitals (top: LUMO, bottom: HOMO) of **10**–**12**.

Time-dependent (TD)-DFT calculations indicated that the HOMO-to-LUMO transitions were dominant in the lowest energy absorption bands observed in UV–Vis spectra. The calculated wavelengths of the lowest transitions at the B3LYP/6-31G* level were λ_{max} = 333, 420, and 482 nm, with oscillator strengths of 0.793, 1.296, and 1.815, for **10**, **11**, and **12**, respectively. The tendency of the bathochromic shift and the enhanced molar coefficients roughly matched with the observed spectra shown in Figure 2. For longer oligomers, the lowest energy transition band was redshifted from 603 nm (for the hexamer) to 659 nm (for the hexadecamer). Although B3LYP function has the tendency to underestimate the molecular excitation, however, the redshift was almost saturated in the dodecamer. Nonetheless, the oscillator strength increased as the number of subunits increased. Although calculation results in the gas phase cannot be directly compared with the solid-state diffuse reflectance spectra owing to the influence of π-stacking being non-neglectable, DFT calculations can roughly explained the diffuse reflectance spectrum of conjugation polymer **17**. As parent polyketone **15** contained very long oligomers, at least docosamer, it was reasonable for conjugated polyimine **17** to exhibit broad and ill-defined absorption bands covering the whole visible region.

CONCLUSIONS

In conclusion, we have developed a two-step transformation of aliphatic polyketones into conjugated polyimines, which results in dramatically changed structural, optical, and coordination properties. As the hydrazine condensation reaction proceeds chemoselectively without forming isolated ketones, all the carbonyl groups were efficiently converted to imine groups. Stereoselective oxidation of the ethylene bridges using *p*-chloranil furnished structurally rigid, π-conjugated compounds that showed significantly redshifted absorption spectra and metal-coordination properties as compared with the starting materials. These transformations were unambiguously confirmed for oligomers **4**–**6** using NMR and X-ray crystallography, and then, applied to polydisperse polymers to give a virtually insoluble organic material with narrow HOMO–LUMO gap. The generation of π-conjugated materials from non-conjugated, and therefore easy-to-handle, precursors is advantageous for the processing of organic π-electronic devices. Furthermore, detailed optimization of the reaction conditions and full characterization of the products with discrete oligomers enabled efficient and reliable transformations of polydisperse polymers to be achieved. Further functionalizations and applications of the polyketone and polyimine materials are in progress in our laboratory.

EXPERIMENTAL SECTION

General information. Solvents and reagents were purchased from WAKO Pure Chemical Industries Ltd., TCI Co., Ltd., and Sigma-Aldrich Co., and used without further purification. All the ^{1}H and $^{13}C\{^{1}H\}$ NMR spectra were recorded using a JEOL JMN-ECS400 (400 MHz) spectrometer at 300 K and the chemical shifts are reported in parts per million (ppm) relative to an internal standard tetramethylsilane (δ = 0.00 ppm for ^{1}H and ^{13}C) in $CDCl_3$. ESI–TOF–MS spectra were recorded on a Thermo Scientific Exactive spectrometer. Infrared spectra were measured using a JASCO Co. FT/IR-4700 spectrometer. Elemental analysis was performed using a CE440 elemental analyzer (Exeter Analytical, Inc.). Single crystal X-ray diffraction data were collected by a Rigaku XtaLAB P200 diffractometer equipped with a PILATUS200K detector using a multi-layer mirror (MoKα radiation λ = 0.71073 Å) or s RAPID II diffractometer with an imaging plate detector. UV–Vis absorption spectra were recorded on a Shimadzu UV-1800 spectrophotometer. Diffuse reflectance spectrum was measured using a JASCO V-670 spectrometer with an integrating sphere unit (JASCO ISN-723). DFT calculations were performed using Gaussian 09 software.[19] MALDI–TOF mass spectra were recorded using Bruker microflex LT MALDI–TOF mass spectrometer. Compounds **2**, **3**, **4**, **6**, **7**, and **9** were prepared according to a reported procedure, but with ethyl acetate used as the extraction solvent in the synthesis of 6 instead of diethyl ether.

*3,3,8,8,13,13-hexamethylpentadecane-2,4,7,9,12,14-hexaone (**5**).* To a 300-mL round-bottom flask equipped with a reflux condenser, were added enol silyl ethers **2** (13.1 g, 65.5 mmol) and **3** (3.57 g, 13.1 mmol), dimethyl sulfone (25.9 g, 275 mmol), dimethyl sulfoxide (1.43 g, 18.3 mmol) and silver(I) oxide (12.8 g, 55.0 mmol). The reaction mixture was stirred at 100 °C for 2 h. After cooling to room temperature, the reaction mixture was passed through a Celite pad using dichloromethane (100 mL). The solvent was evaporated to give the crude products as a brown solid. The solid was dissolved in diethyl ether (100 mL), and the solution was washed with water (100 mL) using an extraction funnel. The aqueous layer was further extracted with diethyl ether (50 mL × 3). The combined organic layer was washed with brine (100 mL), and dried over anhydrous sodium sulfate before evaporating the solvent. The crude product was chromatographed on a silica gel column (diameter, 4.0 cm, height, 15.0 cm) using hexane/ethyl acetate (3:1, v/v) as eluent to give compound **5** (1.35 g, 3.55 mmol) as a colorless solid in 27 % yield based on compound **3**. ^{1}H NMR (400 MHz, $CDCl_3$, 298 K): δ 2.72 (overlapped t, 8H, ethylene), 2.15 (s, 6H, acetyl), 1.41 (s, 6H, dimethylmethylene), 1.37 (s, 12H, dimethylmethylene); ^{13}C{^{1}H} NMR (100 MHz, $CDCl_3$, 298 K): δ 208.6, 208.3, 207.8, 62.3, 61.9, 32.3, 32.2, 26.4, 21.8, 21.7; IR (ATR, neat): 1714, 1693, 1362, 1040, 1014, 970, 504 cm^{-1}; mp 42 ºC; HRMS(ESI-TOF) *m/z*: [*M* + Na]$^+$ Calcd for $C_{21}H_{32}O_6Na$ 403.2089; Found 403.2091; Elemental analysis (%): Calcd for $C_{21}H_{32}O_6$: C, 66.29; H, 8.48; N, 0.00. Found: C, 66.12; H, 8.55; N, 0.04; R_f = 0.24 (eluent: hexane/ethyl acetate = 3:1).

*5,5'-((4,4-dimethyl-4H-pyrazole-3,5-diyl)bis(ethane-2,1-diyl))bis(3,4,4-trimethyl-4H-pyrazole) (**8**).* In a 200-mL round-bottom flask equipped with a reflux condenser, compound **5** (1.70 g, 4.47 mmol) was dissolved in THF (65 mL). Hydrazine monohydrate (780 μL, 16.1 mmol) was then added and the reaction solution was stirred at 50 °C for 30 min. After cooling to room temperature, the solvent was removed using a rotary evaporator to afford the crude product as a white solid. The crude product was dissolved in chloroform (100 mL) and washed with water (100 mL). The aqueous layer was further extracted with chloroform (100 mL × 2). The combined organic layer was dried over anhydrous sodium sulfate, evaporated under reduced pressure, and the obtained solid was then washed with diethyl ether (5 mL) using an ultrasonic bath for 1 min. After filtration, rinsing with diethyl ether (20 mL) on a funnel, compound **8**•0.25(H_2O) (1.45 g, 3.89 mmol) was obtained as a white solid in 87% yield. ^{1}H NMR (400 MHz, $CDCl_3$, 298 K): δ 2.96–3.00 (overlapping (t × 2) + s, 8H, ethylene), 2.15 (s, 6H, terminal methyl), 1.23 (s, 6H, dimethylmethylene), 1.18 (s, 12H, dimethylmethylene); ^{13}C{^{1}H} NMR (100 MHz, $CDCl_3$, 298 K): δ 182.2, 181.8, 180.3, 60.3, 59.9, 22.6, 22.4, 20.5, 20.4, 12.3; IR (ATR, neat): 2971, 2935, 2921, 2889, 2876, 1569, 1465, 1427 cm^{-1}; mp 131-134 ºC (decomp.); HRMS(ESI-TOF) *m/z*: [*M* + H]$^+$ Calcd for $C_{21}H_{33}N_6$ 369.2761; Found 369.2766; Elemental analysis (%): Calcd for $C_{21}H_{32}N_6$•0.25(H_2O): C, 67.62; H, 8.78; N, 22.53. Found: C, 67.79; H, 8.70; N, 22.28; R_f = 0.19 (eluent: dichloromethane/methanol = 10:1).

*(E)-1,2-bis(4,4,5-trimethyl-4H-pyrazol-3-yl)ethene (**10**).* In a 500-mL round bottom flask, compound **7** (1.00 g, 4.06 mmol) and *p*-chloranil (1.10 g, 4.47 mmol) were dissolved in 1,4-dioxane (200 mL) and stirred at room temperature for 1 h. After removing the solvent using a rotary evaporator, the residual solid was dissolved in chloroform (300 mL) and washed with 5% aq. NaOH (100 mL × 3). The organic layer was dried over anhydrous sodium sulfate and evaporated to dryness. The crude product was chromatographed on a silica gel column (diameter, 4.0 cm, height, 5.0 cm) using dichloromethane/methanol (20:1, v/v) as eluent. The resulting solid was then washed with diethyl ether (5 mL) using an ultrasonic bath for 1 min. After filtration, rinsing with diethyl ether (10 mL), compound **10** (866 mg, 3.54 mmol) was obtained as an off-white solid in 87% yield. ^{1}H NMR (400 MHz, $CDCl_3$, 298 K): δ 7.27 (s, 2H, vinylene), 2.23 (s, 6H, terminal methyl), 1.35 (s, 12H, dimethylmethylene); ^{13}C{^{1}H} NMR (100 MHz, $CDCl_3$, 298 K): δ 182.5, 177.4, 126.1, 58.5, 21.1, 12.1; IR (ATR, neat): 3058, 2978, 2937, 2878, 1568, 1523, 1469, 1430, 980 cm^{-1}; mp 199-201 ºC (decomp.); HRMS(ESI-TOF) *m/z*: [*M* + Na]$^+$ Calcd for $C_{14}H_{20}N_4Na$ 267.1580; Found 267.1586; Elemental analysis (%): Calcd for $C_{14}H_{20}N_4$: C, 68.82; H, 8.25; N, 22.93. Found: C, 68.76; H, 8.24; N, 22.75; R_f = 0.09 (eluent: dichloromethane/methanol = 20:1); UV/Vis (dichloromethane): λ_{max} (ε) 309 nm (2.2×10^4 L mol^{-1} cm^{-1}).

*5,5'-((1E,1'E)-(4,4-dimethyl-4H-pyrazole-3,5-diyl)bis(ethene-2,1-diyl))bis(3,4,4-trimethyl-4H-pyrazole) (**11**).* Using the synthetic procedure for compound **10**, compound **11**•0.25(H_2O) (0.77 g, 2.09 mmol) was obtained as a pale yellow solid from **8**•0.25(H_2O) (1.00 g, 2.68 mmol) in 78% yield. ^{1}H NMR (400 MHz, $CDCl_3$, 298 K): δ 7.41 (d, *J* = 17.0 Hz, 2H, vinylene), 7.32 (d, *J* = 17.0 Hz, 2H, vinylene), 2.25 (s, 6H, terminal methyl), 1.53 (s, 6H, dimethylmethylene), 1.36 (s, 12H, dimethylmethylene); ^{13}C{^{1}H} NMR (100 MHz, $CDCl_3$, 298 K): δ 182.6, 179.2, 177.4, 127.2, 125.0, 58.6, 57.4, 22.0, 21.1, 12.3; IR (ATR, neat): 3047, 2993, 2969, 2935, 2871, 1571, 1512, 1459, 1433, 996 cm^{-1}; mp 226-228 ºC (decomp.); HRMS(ESI-TOF) *m/z*: [*M* + H]$^+$ Calcd for $C_{21}H_{29}N_6$ 365.2448; Found: 365.2446; Elemental analysis (%): Calcd for $C_{21}H_{28}N_6$•0.25(H_2O): C, 68.36; H, 7.79; N, 22.78. Found: C, 68.08; H, 7.63; N, 22.42; R_f = 0.24 (eluent: dichloromethane/methanol = 10:1); UV/Vis (dichloromethane): λ_{max}(ε) 363 nm (3.6×10^4 L mol^{-1} cm^{-1}).

*(E)-1,2-bis(4,4-dimethyl-5-((E)-2-(4,4,5-trimethyl-4H-pyrazol-3-yl)vinyl)-4H-pyrazol-3-yl)ethene (**12**).* In a 300-mL round-bottom flask equipped with a reflux condenser, compound **9** (1.00 g, 2.03 mmol) was dissolved in 1,4-dioxane (100 mL) with stirring at 50 ºC using an oil bath. *p*-Chloranil (1.65 g, 6.72 mmol) was then added, and the reaction mixture was stirred for a further 30 min at 50 ºC. After a similar workup to that described in the synthesis of **10**, compound **12**•H_2O (0.74 g, 1.48 mmol) was obtained as a yellow solid in 73% yield. ^{1}H NMR (400 MHz, $CDCl_3$, 298 K): δ 7.46 (s, 2H, vinylene), 7.41 (d, *J* = 17.0 Hz, 2H, vinylene), 7.33 (d, *J* = 17.0 Hz, 2H, vinylene), 2.25 (s, 6H, terminal methyl), 1.53 (s, 12H, dimethyl), 1.36 (s, 12H, dimethylmethylene); ^{13}C{^{1}H} NMR (100 MHz, $CDCl_3$, 298 K): δ 182.7, 179.2, 179.1, 177.4, 127.4, 126.0, 125.0, 58.7, 57.4, 21.9, 21.0, 12.2; IR (ATR, neat): 3048, 2988, 2933, 2873, 1570, 1512, 1459, 1430, 994 cm^{-1}; mp >300 ºC (decomp.); HRMS(ESI-TOF) *m/z*: [*M* + H]$^+$ Calcd for $C_{28}H_{37}N_8$ 485.3136; Found: 485.3134; Elemental analysis (%): Calcd for $C_{28}H_{36}N_8$•(H_2O): C, 66.90; H, 7.62; N, 22.29. Found: C, 67.03; H, 7.26; N, 22.10; R_f = 0.27 (eluent: dichloromethane/methanol = 10:1); UV/Vis (dichloromethane): λ_{max} (ε) 392 nm (5.0×10^4 L mol^{-1} cm^{-1}).

*Cadmium nitrate complex of ethylene-bridged isopyrazole dimer (**13**).* To an acetonitrile solution of $Cd(NO_3)_2$•$4H_2O$ (1.0 mL, 0.30 M) in a 20-mL round-bottom flask was added a solution of ligand **7** (148 mg, 0.60 mmol) in acetonitrile (1 mL). The mixture was stirred for 10 min at room temperature, and then allowed to stand at room temperature. After 3 d, colorless crystals had formed at the bottom of the flask. The crystals were collected by filtration and rinsed with acetonitrile (10 mL) to give complex $[Cd(\mathbf{7})_2(OH_2)_2(NO_3)_2$•$(CH_3CN)]_n$ (106 mg, 0.131 mmol) in 44% yield. IR (ATR, neat): 3365, 3218, 2974, 2935, 2876, 1595, 1577, 1467, 1422, 1386, 1302, 1187, 1114, 1037, 830, 679 cm^{-1}; mp >85 ºC (decomp.); Elemental analysis (%): Calcd for $Cd(C_{14}H_{22}N_4)_2(OH_2)_2(NO_3)_2$•$(CH_3CN)$: C, 44.69; H, 6.38; N, 19.11. Found: C, 44.31; H, 6.26; N, 19.17.

*Cadmium nitrate complex of vinylene-bridged isopyrazole dimer (**14**).* To a 4.0 mM solution of $Cd(NO_3)_2$•$6H_2O$ (136 mg, 0.44

mmol) in acetonitrile (100 mL) in a 300 mL round bottom flask, was added an acetonitrile solution of compound **10** (100 mL, 2.0 mM). After stirring for 15 min at room temperature, brownish microcrystals were precipitated. The precipitate was collected by suction filtration, rinsing with acetonitrile (30 mL), and dried under reduced pressure (1 mmHg) at 100 ºC for 1 h to give Cd complex $[Cd_2(\mathbf{10})(OH_2)_2(NO_3)_4 \cdot 0.25(CH_3CN)]_n$ (**14**) (57 mg) in 37% yield. IR (ATR, neat): 3174, 1584, 1538, 1411, 1389, 1328, 1304, 1043, 970, 818, 740, 714, 683, 659 cm^{-1}; mp >300 ºC (decomp.); Elemental analysis (%): Calcd for $Cd_2(C_{14}H_{20}N_4)(OH_2)_{1.8}(NO_3)_4 \cdot (CH_3CN)_{0.2}$: C, 22.82; H, 3.22; N, 15.16; Found: C, 23.13; H, 3.31; N, 15.19. For powder sample, partial substitution of neutral aqua ligand by solvent acetonitrile which cannot be removed in vacuo was observed.

Supporting Information

The Supporting Information is available free of charge on the ACS Publications website at DOI:

NMR spectra, X-ray structure, DFT calculations, powder X-ray data, synthesis and characterization of polymer materials (PDF)
X-ray Crystallographic data for compound **5** (CIF)
X-ray Crystallographic data for compound **10** (CIF)
X-ray Crystallographic data for compound **11** (CIF)
X-ray Crystallographic data for complex **13** (CIF)
X-ray Crystallographic data for complex **14** (CIF)

AUTHOR INFORMATION

Corresponding Author

*E-mail: inokuma@eng.hokudai.ac.jp

Author Contributions

The manuscript was written through contributions of all authors.

ORCID

Y. Inokuma: 0000-0001-6558-3356

Notes

The authors declare no competing financial interest.

ACKNOWLEDGMENT

This work was supported by Grant-in-Aid for Young Scientists (A) (No. 17H04872), and by the Asahi Glass Foundation. We thank Prof. Dr. Yasuchika Hasegawa, Dr. Yuichi Kitagawa, and Mr. Ferreira da Rosa Pedro Paulo for measurement of diffuse reflectance spectrum.

REFERENCES

(1) (a) Hertweck, C. The Biosynthetic Logic of Polyketide Diversity. *Angew. Chem. Int. Ed.*, **2009**, *48*, 4688-4716. (b) Rubin, M. B.; Gleiter, R. The Chemistry of Vicinal Polycarbonyl Compounds. *Chem. Rev.* **2000**, *100*, 1121-1164. (c) Harris, T. M.; Harris, C. M. Synthesis of polyketide-type aromatic natural products by biogenetically modeled routes. *Tetrahedron*, **1977**, *33*, 2159-2185. (d) Sommazzi, A.; Garbassi, F. Olefin-carbon monoxide copolymers. *Prog. Polym. Sci.* **1997**, *22*, 1547-1605. (e) Yang, Y.; Li, S.-Y.; Bao, R.-Y.; Liu, Z.-Y.; Yang, M.-B.; Tan, C.-B.; Yang, W. Progress in polyketone materials: blends and composites. *Polym. Int.* **2018**, *67*, 1478-1487.

(2) (a) Rahn, T.; Bendrath, F.; Hein, M.; Baumann, W.; Jiao, H.; Börner, A.; Villinger, A.; Langer, P. Synthesis and characterization of bis-cyclopropanated 1,3,5-tricarbonyl compounds. A combined synthetic, spectroscopic and theoretical study. *Org. Biomol. Chem.* **2011**, *9*, 5172-5184. (b) Alder, R. W.; Hyland, N. P.; Jeffery, J. C.; Riis-Johannessen, T.; Riley, D. J. Poly(1,1-bis(dialkylamino)propan-1,3-diyl)s; conformationally-controlled oligomers bearing electroactive groups. *Org. Biomol. Chem.* **2009**, *7*, 2704-2715. (c) Peter, M.; Gleiter, R.; Rominger, F.; Oeser, T. A Cyclic Vicinal Bis(tetraketone) and Structural Investigations of Formoins. *Eur. J. Org. Chem.* **2004**, 3212-3220. (d) Harris, T. M.; Hay, J. V. Biogenetically modeled syntheses of heptaacetate metabolites. Alternariol and lichexanthone. *J. Am. Chem. Soc.* **1977**, *99*, 1631-1637. (e) Pregaglia, G. F.; Binaghi, M. Formation of 2,2,4,4,6,6-Hexamethyl-1,3,5-cyclohexanetrione from Dimethylketene and from Its Polymers. *J. Org. Chem.* **1963**, *28*, 1152-1154.

(3) (a) Zhang, Y.; Broekhuis, A. A.; Picchioni, F. Thermally Self-Healing Polymeric Materials: The Next Step to Recycling Thermoset Polymers? *Macromolecules* **2009**, *42*, 1906–1912. (b) Cheng, C.; Guironnet, D.; Barborak, J.; Brookhart, M. Preparation and Characterization of Conjugated Polymers Made by Postpolymerization Reactions of Alternating Polyketones. *J. Am. Chem. Soc.* **2011**, *133*, 9658-9661.

(4) Uesaka, M.; Saito, Y.; Yoshioka, S.; Domoto, Y.; Fujita, M.; Inokuma, Y. Oligoacetylacetones as shapable carbon chains and their transformation to oligoimines for construction of metal-organic architectures. *Comms. Chem.* **2018**, *1*, 23.

(5) Yi-Shan, S.; Boobalan, R.; Chen, C.; Lee, G.-H. Novel C_2-symmetric chiral *O,N,N,O*-tetradentate 2,2-bipyridyldiolpropane ligands: synthesis and application in asymmetric diethylzinc addition to aldehydes. *Tetrahedron Asymmet.* **2014**, *25*, 327-333.

(6) Ito, Y.; Konoike, T.; Saegusa, T. Synthesis of 1,4-diketones by the reaction of silyl enol ether with silver oxide. Regiospecific formation of silver(I) enolate intermediates. *J. Am. Chem. Soc.* **1975**, *97*, 649-651.

(7) Cafeo, G.; Garozzo, D.; Kohnke, F. H.; Pappalardo, S. Parisi, M. F. Nascone, R. P. Williams, D. J. From calixfurans to heterocyclophanes containing isopyrazole units. *Tetrahedron*, **2004**, *60*, 1895-1902.

(8) When exposed to air (humidity ~25%) at room temperature, weight of anhydrous compound **7** increased 10% after 1 week.

(9) (a) Kötzner, L.; Webber M. J.; Martínez, A.; De Fusco, C.; List, B.; *Angew. Chem. Int. Ed.* **2014**, *53*, 5202-5205. (b) Sakikumar, M.; Bharatha. D.; Kumar, G. S.; Chereddy N. R.; Chithiravel S.; Krishnamoorthy, K.; Shanigaram, B.; Bhanuprakash K.; Rao, V. J. Role of acceptor strength on OFET properties of small molecular organic semiconducting materials with D-A-D architecture *Syn, Metals.* **2016**, *220*, 236 (c) Sivakumar, G. Sasikumar, M. Rao. V. J. Synthesis and Characterization of Diketopyrrolopyrrole-based D-π-A-π-D Small Molecules for Organic Solar Cell Application. *J. Heterocyclic Chem.* **2017**, *54*, 1983-1994. (d) Yoneda, T.; Hoshino, T.; Neya, S. [24]Pentaphyrin(2.1.1.1.1): A Strongly Antiaromatic Pentaphyrin, *J. Org. Chem.* **2017**, *82,* 10737.

(10) Crystallographic data for **10**: $[C_{14}H_{20}N_4]$, M =244.34, crystal size: 0.45 × 0.31 × 0.09 mm^3, monoclinic, space group $P2_1/n$, a = 6.1286(4) Å, b = 12.4667(8) Å, c = 9.5271(8) Å, β = 104.044(8)º, V = 706.15(9) $Å^3$, Z = 2, T = 123(2) K, μ = 0.071 mm^{-1}, D_{calc} = 1.149 g/cm^3, 2.743º ≤ θ ≤ 25.990º, 1149 unique reflections out of 1381 with $I > 2\sigma(I)$, GOF = 1.100, R_1 = 0.0439 and wR_2 = 0.1106 for all data. (CCDC number: 1905112).

(11) Crystallographic data for **11**: $[C_{21}H_{28}N_6]$, M =364.49, crystal size: 0.45 × 0.23 × 0.02 mm^3, monoclinic, space group $P2/c$, a = 15.1672(15) Å, b = 6.1734(6) Å, c = 10.7592(11) Å, β = 98.628(9)º, V = 996.02(17) $Å^3$, Z = 2, T = 123(2) K, μ = 0.076 mm^{-1}, D_{calc} = 1.215 g/cm^3, 2.717º ≤ θ ≤ 24.995º, 1426 unique reflections out of 1769 with $I > 2\sigma(I)$, GOF = 1.107, R_1 = 0.0474 and wR_2 = 0.1409 for all data. (CCDC number: 1905113).

(12) Blout, E. R.; Fields, M. Absorption Spectra. V. The Ultraviolet and Visible Spectra of Certain Polyene Aldehydes and Polyene Azines. *J. Am. Chem. Soc.* **1940**, *70*, 189-193.

(13) Ashida, Y.; Manabe, Y.; Yoshioka, S.; Yoneda, T.; Inokuma, Y. Control over coordination self-assembly of flexible, multidentate ligands by stepwise metal coordination of isopyrazole subunits. *Dalton Trans.* **2019**, *48*, 818-822.

(14) Crystallographic data for **13**: $[Cd(C_{14}H_{22}N_4O)_2(NO_3)_2 \cdot (H_2O)_2(CH_3CN)_2]$, M =847.27, crystal size: 0.35 × 0.14 × 0.09 mm^3, tetragonal, space group $P4/n$, a = 15.0815(18) Å, b = 15.0815(18) Å, c = 8.9943(6) Å, $\alpha = \beta = \gamma$ = 90º, V = 2045.8(5) Å^3 , Z = 2, T = 143(2) K, μ = 0.594 mm^{-1}, D_{calc} = 1.375 g/cm^3, 1.910º ≤ θ ≤ 27.431º, 2210 unique reflections out of 2348 with $I > 2\sigma(I)$, GOF = 1.040, R_1 = 0.0287 and wR_2 = 0.0713 for all data. (CCDC number: 1905114).

(15) Powder X-ray diffraction analysis confirmed that microcrystals obtained from acetonitrile show the same diffraction pattern to that of single crystals grown from ethanol (see SI).

(16) Wei, C. H.; Jacobson, K. B. X-ray crystallographic characterization of an adenine-cadmium(II) complex, di-.mu.-adeninium-di-.mu.-aquo-tetrakis(nitrato-O,O')dicadmium(II) dinitrate, containing a cationic nucleic acid base as a bidentate ligand. *Inorg. Chem.* **1981**, *20*, 356-363.

(17) Crystallographic data for **14**: $[(C_{14}H_{20}N_4Cd_2)(NO_3)_4 \cdot (H_2O)_2]$, M = 376.61, crystal size: 0.14 × 0.03 × 0.03 mm^3, monoclinic, space group $C2/m$, a = 10.1187(6) Å, b = 12.0670(7) Å, c = 10.3366(6) Å, β = 94.727(5)º, V = 1257.83(13) Å^3 , Z = 4, T = 123(2) K, μ = 1.773 mm^{-1}, D_{calc} = 1.989 g/cm^3, 2.632º ≤ θ ≤ 26.492º, 1249 unique reflections out of 1363 with $I > 2\sigma(I)$, GOF = 1.127, R_1 = 0.0291 and wR_2 = 0.0780 for all data. (CCDC number: 1905115).

(18) Fleming, I. *Molecular Orbitals and Organic Chemical Reactions Reference Edition*, John Wiley & Sons, Ltd, Chichester, West Sussex, UK, **2010**, pp. 1-66.

(19) Gaussian 09, Revision D.01, Frisch, M. J.; Trucks, G. W.; Schlegel, H. B.; Scuseria, G. E.; Robb, M. A.; Cheeseman, J. R.; Scalmani, G.; Barone, V.; Petersson, G. A.; Nakatsuji, H.; Li, X.; Caricato, M.; Marenich, A.; Bloino, J.; Janesko, B. G.; Gomperts, R.; Mennucci, B.; Hratchian, H. P.; Ortiz, J. V.; Izmaylov, A. F.; Sonnenberg, J. L.; Williams-Young, D.; Ding, F.; Lipparini, F.; Egidi, F.; Goings, J.; Peng, B.; Petrone, A.; Henderson, T.; Ranasinghe, D.; Zakrzewski, V. G.; Gao, J.; Rega, N.; Zheng, G.; Liang, W.; Hada, M.; Ehara, M.; Toyota, K.; Fukuda, R.; Hasegawa, J.; Ishida, M.; Nakajima, T.; Honda, Y.; Kitao, O.; Nakai, H.; Vreven, T.; Throssell, K.; Montgomery, J. A. Jr.; Peralta, J. E.; Ogliaro, F.; Bearpark, M.; Heyd, J. J.; Brothers, E.; Kudin, K. N.; Staroverov, V. N.; Keith, T.; Kobayashi, R.; Normand, J.; Raghavachari, K.; Rendell, A.; Burant, J. C.; Iyengar, S. S.; Tomasi, J.; Cossi, M.; Millam, J. M.; Klene, M. Adamo, C.; Cammi, R.; Ochterski, J. W.; Martin, R. L.; Morokuma, K.; Farkas, O.; Foresman, J. B.; Fox, D. J. Gaussian, Inc., Wallingford CT, 2016.

Table of Content